

# Proton Shuttle Mechanism for the Oxidation of Formaldehyde by Aldehyde Oxidase: An Electronic Structure Description of Formal Hydride Transfer and “Inhibited” Species

Tadege Belay <sup>#1</sup>, Dr. Abebe Berhane <sup>\*2</sup>

<sup>#</sup>Tadege Belay, South Gonder (Debre Tabor University), Debre Tabor, Ethiopia.

## Abstract

The mechanism(s) of molybdoenzymes such as aldehyde oxidase and xanthine oxidase is of interest since these enzymes are more frequently being linked to major metabolic pathways of drugs. Aldehyde oxidase(AO) enzyme is known to oxidize aldehydes. One of the aldehydes, formaldehyde, is known to inhibit xanthine oxidase as it turns over. However, there is no reported data whether it behaves the same when it reacts with aldehyde oxidase. Therefore, the research is intended to probe the most plausible proton shuttle mechanism for the oxidation of formaldehyde that precedes through either a concerted or stepwise mechanism. Density Functional Theory of the B3LYP correlation functional formalism (DFT-B3LYP) methods were used to generate several parameters from the electronic structure calculations. Accordingly, the higher percentage (%) contribution to HOMO and energy barrier (kcal/mol) (0.099, -7.185040E+04) makes formaldehyde as the favored substrate for aldehyde oxidase. In addition, the transition state structures for the active site bound to formaldehyde (ACT-FA) was confirmed by one imaginary negative frequency(-328.44S<sup>-1</sup>). Similarly, the wave function and bonding description support a stepwise formal hydride transfer mechanism (Path IC) for the oxidation of formaldehyde.

**Keywords:** Aldehyde oxidase (AO), formaldehyde (FA), proton shuttle, oxidative hydroxylation, DFT-B3LYP

## I. INTRODUCTION

One of the fascinating and commonly used metals in life is molybdenum, which serves as a cofactor for enzymes. It is needed as a catalytically active metal during enzyme catalysis of most living systems [1], [2], [3]. Aldehyde oxidase (AO) is the most prevalent families of an enzyme in living systems involved in the conversion of formaldehyde to formate, which is formed continuously in various biological processes. AO is involved in the metabolism of a wide range of endogenous compounds and many drug substances. It undergoes oxidative and reductive half-reactions. It can oxidize a wide range of substrates including aldehydes and N-heterocyclic compounds. Aldehyde Oxidase has a physiological, biological, medicinal, mechanistic, and toxicological significance. Because of the various signs of xanthine oxidase family enzyme, aldehyde oxidase has attracted the attention of many researchers to study their mechanistic actions [4].

### A. The Mechanism Action of Aldehyde Oxidase

A better understanding of the overall mechanism should enhance the ability to control the metabolic properties of potential drug molecules metabolized by these enzymes. One of the postulated mechanisms, proposed for AO enzymes, is based on a base-assisted nucleophilic attack by the HO<sub>eq</sub> terminal at the electron deficient carbon of the substrates [5].

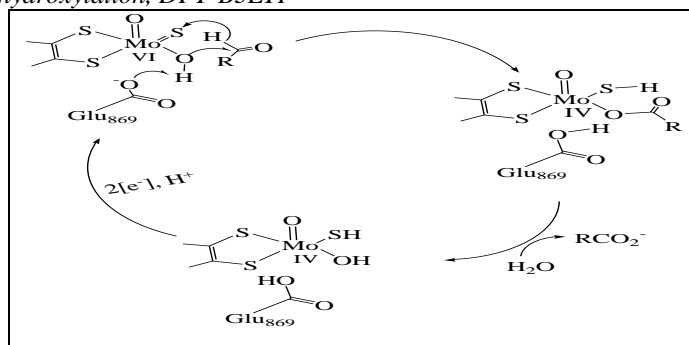


Fig 1.1: A postulated base-assisted hydride transfer mechanism for the aldehyde oxidase [5].

As described by R. Hille (2005), the reaction mechanisms for oxidative hydroxylation of aldehydes by AO enzyme are proposed to take place through a base-assisted nucleophilic reaction [6]. However, the

mechanism of action of AO is not well understood. In order to understand the mechanism of action, proton shuttle mechanistic routes are proposed as shown in Fig.1.2 and Fig.1.3.

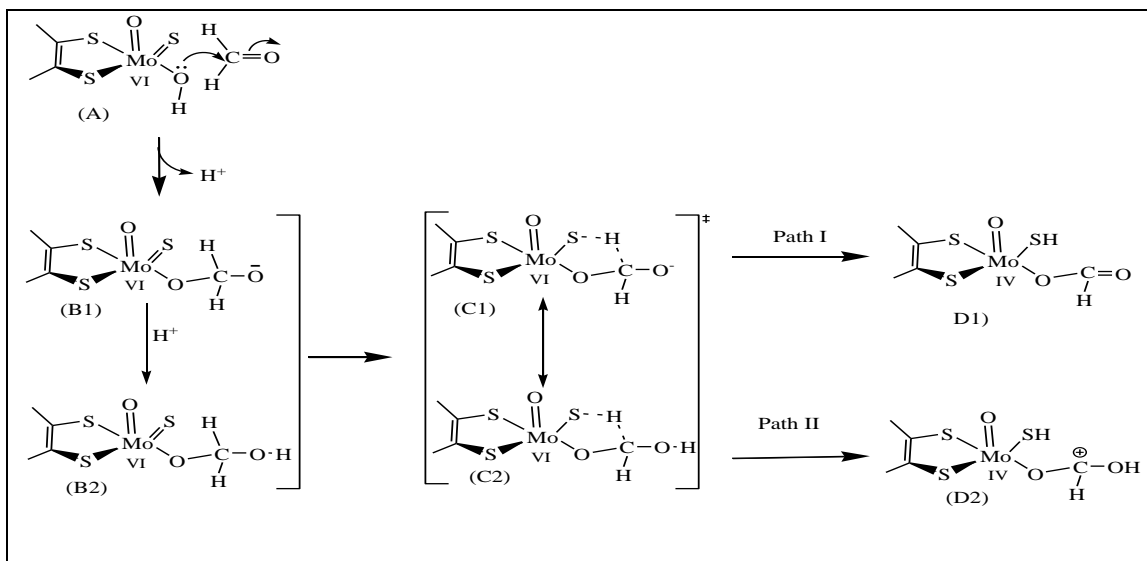
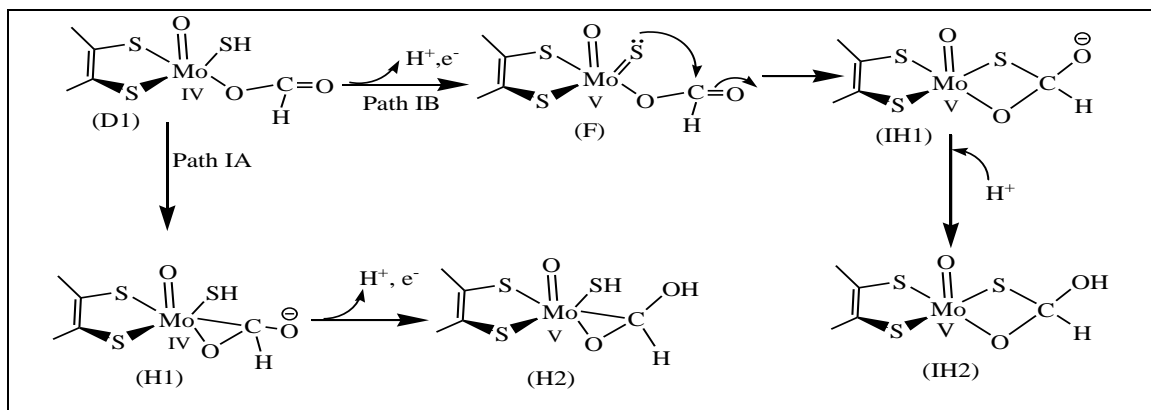
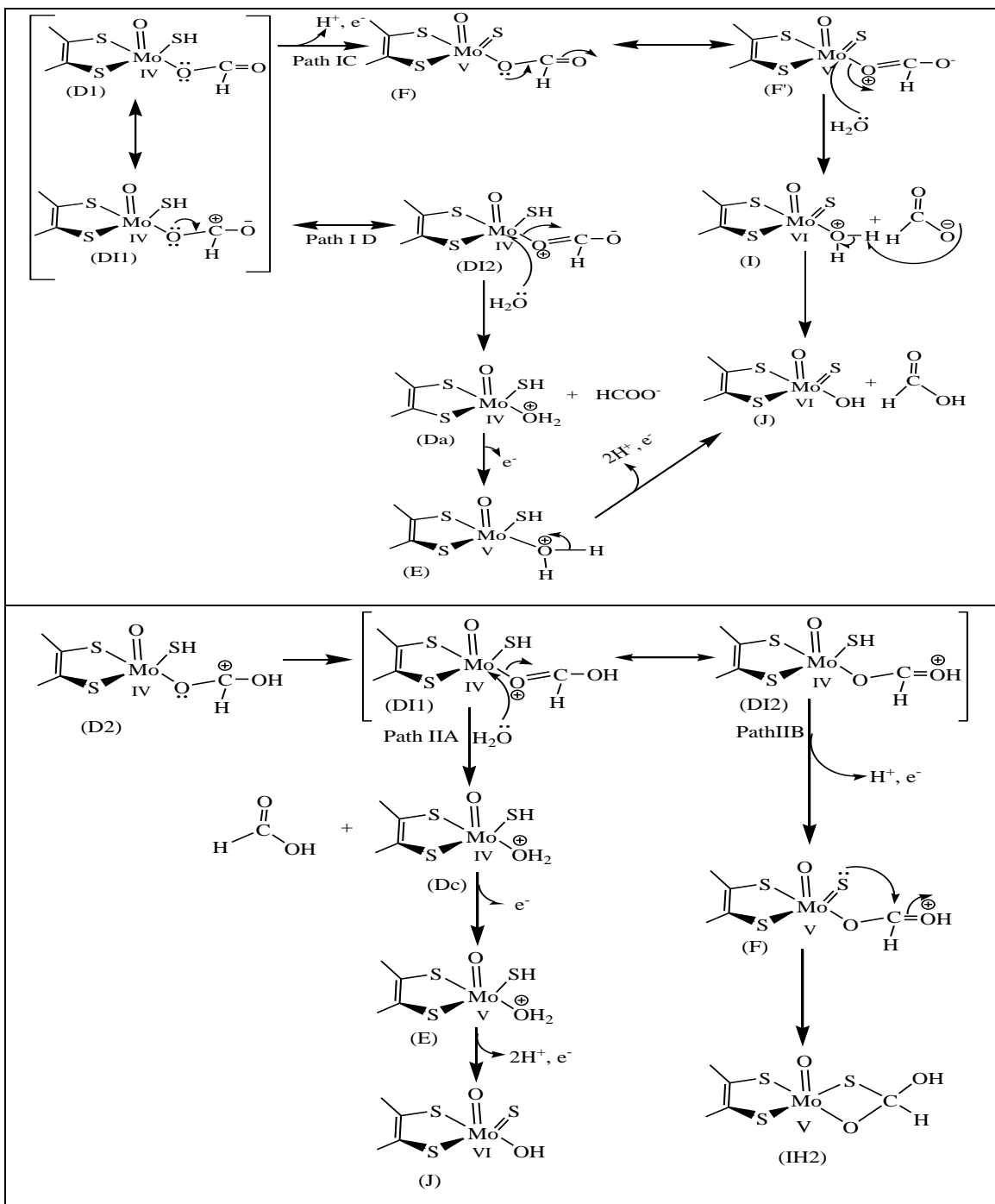


Fig 1.2: The proposed mechanistic route for the initial stage of catalysis showing deprotonated (D) and protonated (P) FA bound to AO (ACT-FA). The designation (A, B1, B2, C1, C2, D1, and D2) indicates the structures developed from the proton shuttle mechanism. Where, A = is the near attack conformation (resting state), B1 and B2, respectively, are deprotonated and Protonated FA bound Michaelis menten type complex; C1 (ACT-D FA) and C2 (ACT-UP FA), respectively, are deprotonated and protonated transition state structures; D1 and D2 respectively, represents deprotonated and protonated Mo<sup>IV</sup> product bound intermediates.

The Michaelis-Menten type complex (B1 and B2) enters into the transition state (C1 and C2), respectively. The reaction mechanism proceeds either through the deprotonated (C1) or protonated (C2) transition state structure, as shown in Fig.1.2. The events taking place at the transition state (C1 and C2) have never been fully explored nor quite understood. Most importantly, the transition state structure has not been established to date. The geometry of the transition state structure is

central in understanding the catalytic reaction mechanism although the smallest fraction of the catalytic cycle is spent in the transition state. However, the implication of protonation and deprotonation of the substrate (formaldehyde) on the reaction mechanism and the nature of products generated have never been studied. In addition, different mechanistic routes were also proposed for the oxidation of formaldehyde by aldehyde oxidase (Fig. 1.3).





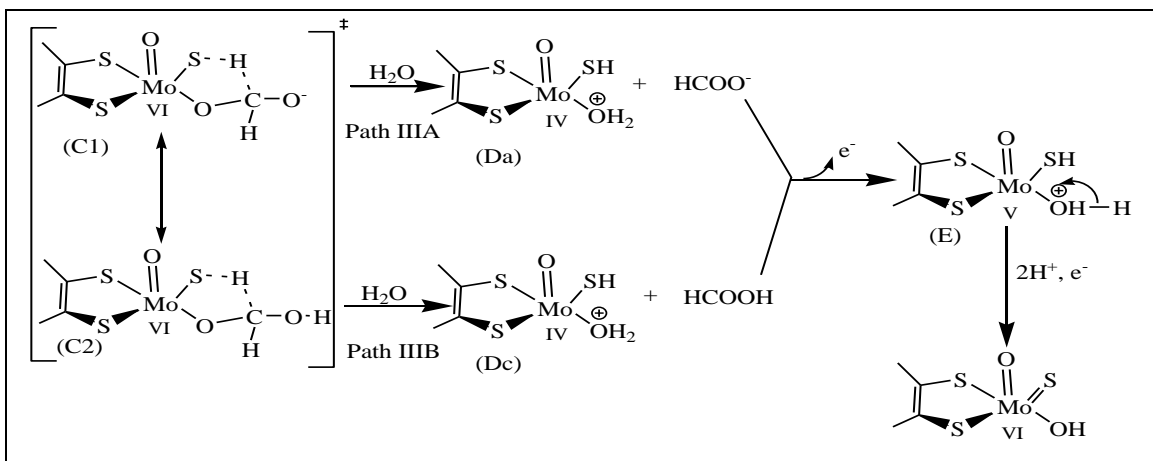


Fig 1.3: The proposed mechanistic route for the oxidation of FA by AO that passes through the deprotonated transition state structure (developed from Fig 1.2). The symbol (Da, E, F, F', I, J, IH1, H1, IH2, and, H2) indicates the labels of the intermediates. Where, Da is water coordinated  $\text{Mo}^{\text{IV}}\text{-SH}$  intermediate including formate ion, DI1 and DI2 are  $\text{Mo}^{\text{IV}}\text{-SH}$  product bound, E is protonated water coordinated  $\text{Mo}^{\text{V}}\text{-SH}$  complex, F is  $\text{Mo}^{\text{V}}\text{-S}$  product bound, F' is  $\text{Mo}^{\text{V}}\text{-S}$  product bound, I is water coordinated  $\text{Mo}^{\text{VI}}$  complex, J is product released  $\text{Mo}^{\text{VI}}$ , IH1 is inhibited  $\text{Mo}^{\text{V}}\text{-S}$  complex, IH2 is inhibited  $\text{Mo}^{\text{V}}\text{-S}$  product, and H2 is inhibited  $\text{Mo}^{\text{V}}\text{-SH}$  product.

Therefore the work is intended to probe whether the structure entering the transition state is in the form of carbonyl (deprotonated) or hydrated (protonated) bound to the active site (Fig.1.2). For both protonated and deprotonated formaldehyde bound to the active site, the variation in bonding and wave function description is expected to provide a clue whether the formation and dissociation of the tetrahedral transition state complex take place in a concerted or stepwise mechanistic pathway. Finally, the work is expected to give a clue whether the protonated and deprotonated forms provide a product or an inhibited structure via a concerted or stepwise mechanistic pathway.

In order to achieve the desired objectives, computation approaches have been designed. Thus, the computation approach helps to evaluate the electronic structure and wave function descriptions of the geometries produced during the overall mechanistic transformation. All computation calculations, for the geometries shown in Fig.1.2 and Fig.1.3, were carried out by applying Density functional theory (DFT) of the B3LYP (Becke3- Lee-Yang-Parr) correlation functional formalism (DFT-B3LYP) methods [7]. All calculations were performed using Gaussian software Packages. Several parameters were expected to be generated (such as the electronic energies, Mulliken atomic charges, and bonding and wave function descriptions). The transition state structures were characterized by one imaginary negative frequency. The bonding descriptions were provided in terms of atomic charges, bond distance and bond order. The bonding descriptions were used to quantitative the formation of  $\text{O}_{\text{eq}}\text{-C}_{\text{CRH}}$  and  $\text{S}_{\text{Mo}}\text{-H}_{\text{RH}}$  and cleavage of  $\text{C}_{\text{CRH}}\text{-H}_{\text{RH}}$  and  $\text{Mo-O}_{\text{eq}}$  bonds. Because the  $\text{C}_{\text{CRH}}\text{-H}_{\text{RH}}$  bond distance varied significantly, during the formation of  $\text{O}_{\text{eq}}\text{-C}_{\text{RH}}$  bond, the position of  $\text{H}_{\text{RH}}$  and

cleavage of  $\text{C}_{\text{CRH}}\text{-H}_{\text{RH}}$  bond were proposed to depend on the nature of the substrates.

Upon the completion of this work, key questions regarding the implication of deprotonation/protonation of formaldehyde on the product release stage, and the events taking place at the transition state were expected to be answered.

The goal of this work was to provide a more complete understanding of the oxidative hydroxylation of formaldehyde by the reductive half-reaction active site of AO and probing the most plausible mechanistic transformations to develop a unified reaction mechanism. Generally, the theoretical work was expected to relate electronic structure contributions to enzymatic catalysis and provide a deeper mechanistic insight into the enzyme-catalyzed reactions.

## II. MATERIALS AND METHODS

### A. Materials

The software packages that were used for the completion of the study were GaussView 3.0 (Gaussian, Inc., Pittsburgh PA, USA), Gaussian 03W version 6.0 (Gaussian, Inc., Wallingford, CT, U.S.A), AOMix 2011/2012 version 6.6 (Centre for Catalysis Research and Innovation, the University of Ottawa), Chem Draw Ultra, version 8.0 (Cambridge soft corp., Cambridge, MA, USA), Dell computer Optiplex 780 model, 2011 (Dell, Inc., Wilhile Sdhbhd., Penang, Malaysia), Microsoft Excel 2003/2007 and word 2007 (Microsoft, Inc., Redmond, Washington, U.S.A). The Chem Draw Ultra, version 8.0 was used to draw/sketch the structures and mechanisms. The structures (geometries) were constructed and input geometries for geometry optimization were prepared using GaussView 3.0

software package. In addition, the GaussView software was also used to compute the bond distances from the output geometries of the optimized structures and visualize pictorial view of frontier orbitals generated from checkpoint files. All computation calculations were performed using Gaussian 03W (version 6.0) program software package. The molecular orbital analyses for the constituent chemical fragments were performed using AOMix 2011/2012 version 6.6 software package. These analyses were performed from the output files obtained from the single point energy calculations. Finally, Microsoft Excel, powerpoint and Word were used for data handling, and research writes up. All calculations and write-up were carried out on Dell Computer.

### B. Methods

Electronic structure calculations were performed to generate Mulliken atomic charges, total electronic energies, wave function description, and bonding descriptions. All computation calculations were carried out by applying the density functional theory (DFT) method of the B3LYP (Becke3-Lee-Yang-Parr) correlation functional formalism (DFT-B3LYP) using the Gaussian 03W (version 6.0) program software packages [8, 9]. The 6-31G (d', p') basis set with a polarization function was applied for non-metal atoms (C, H, O, and S). Similarly, the LANL2DZ (Los Alamos National Laboratory 2 Double Zeta) basis set and LANL2 effective core potentials were applied for Mo atoms [8, 10]. The DFT method employing the B3LYP level of theory was applied to different structures shown in Fig.1.2 and Fig.1.3. In all types of linear transit scan, geometry optimization, frequency, single point energy, and transition state search calculations, the "# b3lyp gen pseudo=read #p gfinput pop=full gfp rint" general keywords and job type were

used. In all calculations, the general job type and key words were used by applying other key words relevant to the respective calculations.

### C. Computational Detail

**Proton shuttle mechanism for the oxidation of formaldehyde:** In order to develop a more general mechanism for aldehyde oxidase enzymes computational method has been developed to perform electronic structure calculations at DFT/B3LYP on the geometries shown in Fig. 1.2 and Fig.1.3. The total electronic energy, bond order, wave function, percent contribution of chemical fragments and Mulliken atomic charge of atoms ( $M_o$ ,  $O_{eq}$ ,  $C_{RH}$ ,  $H_{RH}$ ,  $S_{Mo}$ ) are expected to give an insight to the general mechanism. The geometries representing the tetrahedral transition state structures (C1 and C2) were modeled by placing the substrate bound hydrogen ( $H_{RH}$ ) between the sulfido terminal ( $S_{Mo}$ ) and the carbon atom of the substrate ( $C_{RH}$ ) as shown in Fig.1.3.

A series of geometry optimizations were carried out by stepping up or down the substrate hydrogen ( $H_{RH}$ ) between  $C_{RH}$  and  $S_{Mo}$ , at constant intervals of (1.3323 Å). The substrate hydrogen ( $H_{RH}$ ) was fixed at (1.19708 Å) from substrate carbon ( $C_{RH}$ ) and (2.04231 Å) from the  $S_{Mo}$  as well as the typical C-H (1.09Å, in methanol) and the typical S-H (1.35Å, in thiol or sulfhydryl group) bond distances were subtracted from substrate carbon atom and  $S_{Mo}$ , respectively. This helps to know the possible distances that the substrate hydrogen moves either towards to  $S_{Mo}$  or  $C_{RH}$ . The  $S_{Mo}$ - $C_{RH}$  bond distance was divided into seven runs including the initial position of  $H_{RH}$  by stepping up five trials and stepping down one trial at constant interval of (0.13323 Å), as shown in Table 2.1.

Table 2.1: The  $S_{Mo}$ - $H_{RH}$  Distances Used to Optimize the Structure During the Linear Transit Calculation of ACT-D FA (Fig. 1.2 (C1)). The Same Calculation was Performed for ACT-P FA (Fig. 1.2, C2).

Run	1	2	3	4	5	6	7
$S_{Mo}$ - $H_{RH}$ distance in (Å)	1.37616	1.50939	1.64262	1.77585	1.90908	2.04231	2.17554

All input geometries were prepared by fixing  $S_{Mo}$ - $H_{RH}$  bond distances shown in Table 2.1 using GaussView software package. All linear transit calculations were carried out at  $Mo^{VI}$  oxidation state. Once a series of geometry optimizations were carried out, the total energy from each optimization was plotted against respective  $S_{Mo}$ - $H_{RH}$  bond distances. The geometry with the highest energy was considered as initial guess for the transition structure search. The optimized structures (from substrate bound, product bound, and the initial guess) were assembled as input geometries for the transition state (TS) search

calculation. The transition state structure search was carried out by applying "iop(6/7=3) Opt=QST3" keyword. The "QST3" (quadratic synchronous transit method) keyword was used to search the transition state structure on the structures containing three input files (substrate bound, initial guess, and product-bound). The frequency calculations on the optimized structure from the transition state search were carried out by applying the "freq" keyword. The frequency calculations were used to distinguish the one negative imaginary frequency. The molecular orbital analyses for the constituent chemical fragments were performed using

AOMix 2011/2012 version 6.6 software package from the single point energy calculation outputs.

### III. RESULTS AND DISCUSSION

As described in the introduction section, understanding the mechanistic pathways in the presence of different substrates was of considerable mechanistic interest. The reaction mechanisms for the oxidative hydroxylation of aldehydes by AO enzyme was proposed to take place through a base-assisted nucleophilic reaction [5]. In this work, different mechanistic routes were proposed for the oxidative hydroxylation of FA by AO as shown in the introduction section (Fig. 1.2 and 1.3). The electronic structure calculations were performed in order to predict

the reasonable mechanistic routes for the oxidative hydroxylation of FA by AO. The parameters from electronic structure calculations such as total energies, Mulliken atomic charges, bond distance, the percentage composition of the constituent chemical fragments, and the frontier orbitals were assembled.

#### A. Proton Shuttle Mechanism for the Oxidation of Formaldehyde

##### 1. Prediction of the Mechanistic Route during the Initial and Catalysis Stages

The normalized activation energies with respect to structure (A); the interaction between deprotonated (D) and protonated (P) FA and active site were shown in Fig. 3.1.

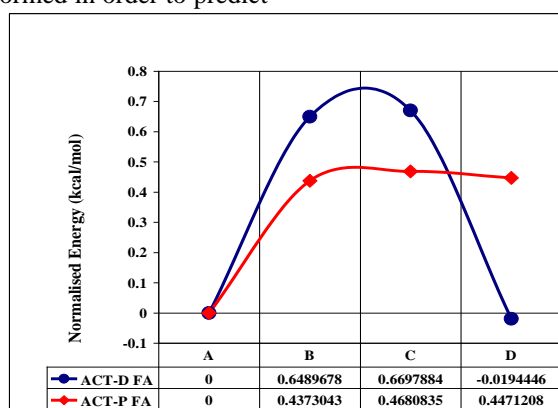


Fig 3.1: The normalized total energy difference obtained in the presence of D FA and P FA, respectively, bound to the truncated reductive half-reaction active site of AO (ACT-D FA and ACT-P FA).

The activation barriers for ACT-D FA and ACT-P FA, respectively, were calculated to be 0.6697884 and 0.468084 kcal/mol. The activation energy of the substrate bound intermediate (B) for ACT-D FA was higher by 0.212 kcal/mol than for ACT-P FA which reflected the effect of stability of the substrate bound intermediate. Therefore, the protonated formaldehyde bound intermediate featured a strong covalent metal-substrate interaction [11]. Moreover, formaldehyde exhibited lower energy than the protonated formaldehyde during the conversion of reactants to the corresponding products (D). It should be noted that the protonation of formaldehyde led to a much less stable product (Fig.3.1). As a result, the oxidative hydroxylation of formaldehyde by aldehyde oxidase yielded a thermodynamically stable product. Therefore,

the protonation of formaldehyde had different connotation on the rate of the reaction and the nature of product generated throughout the reaction. The oxidative hydroxylation reaction was supported by the proton shuttle mechanism. Thus, the proton transfer reaction was essential for the high activity of the enzyme towards the substrate (FA). Because, it increased the nucleophilicity of the migrating catalytically labile equatorial oxygen ( $O_{eq}$ ) and strengthened the electrophilicity of the target C-atom ( $C_{RH}$ ) of the substrate (FA), the formation of substrate-bound intermediate (B) was feasible. The bond distance ( $Mo-S_{Mo}$ ,  $Mo-O_{eq}$ ,  $S_{Mo}-H_{RH}$ ,  $O_{eq}-C_{RH}$ , and  $C_{RH}-H_{RH}$ ) and Mulliken atomic charge on selected atoms ( $Mo$ ,  $S_{Mo}$ ,  $O_{eq}$ ,  $C_{RH}$ , and  $H_{RH}$ ) involved in the redox reactions were shown in Table 3.1.

Table 3.1: The Bond Distance (Å) and Mulliken Atomic Charge (A.U) Description of Selected Atoms for D FA and P FA Bound to the Reductive Half-Reaction Active Site of Aldehyde Oxidase.

Structures	Bond Distance (Å)					Mulliken Atomic charge (a.u)				
	ACT-D FA					ACT-D FA				
	Mo- $S_{Mo}$	Mo- $O_{eq}$	$S_{Mo}$ - $H_{RH}$	$O_{eq}$ - $C_{RH}$	$C_{RH}$ - $H_{RH}$	Mo	$S_{Mo}$	$O_{eq}$	$C_{RH}$	$H_{RH}$

<b>A</b>	2.1881	1.9721	2.8791	2.6761	1.1084	0.66124	-0.4155	-0.6046	0.11575	0.09112
<b>B</b>	2.2399	1.7617	2.8199	2.5873	1.1140	0.62070	-0.6249	-0.5890	0.10281	0.10563
<b>C</b>	2.2466	1.8944	1.5579	1.5579	1.1965	0.60437	-0.4952	-0.5707	0.24583	0.01632
<b>D</b>	2.4783	2.1769	1.3585	1.2872	2.7393	0.40208	-0.3937	-0.4369	0.26589	-0.01978
	<b>ACT-P FA</b>					<b>ACT-P FA</b>				
<b>A</b>	2.1881	1.9721	2.8791	2.6761	1.10846	0.66124	-0.4155	-0.6046	0.11575	0.09112
<b>B</b>	2.1839	1.9780	2.8337	1.3928	1.10449	0.62410	-0.3952	-0.5513	0.20345	0.08341
<b>C</b>	2.3011	2.0702	1.5966	1.2877	1.43190	0.51482	-0.2814	-0.4290	0.22629	-0.02850
<b>D</b>	2.4552	2.3526	1.3576	1.2093	3.48081	0.35771	-0.3013	-0.2664	0.29955	-0.01286

As shown in Table 3.1, the bond distances of Mo-S<sub>Mo</sub> and C<sub>RH</sub>-H<sub>RH</sub> was increased, while the other bond distances (S<sub>Mo</sub>-H<sub>RH</sub> and O<sub>eq</sub>-C<sub>RH</sub>) were decreased during the reduction of Mo from Mo<sup>VI</sup> to Mo<sup>IV</sup> in the oxidative hydroxylation of both D FA and P FA by aldehyde oxidase. The lengthening of Mo-S<sub>Mo</sub> and C<sub>RH</sub>-H<sub>RH</sub>, respectively, was due to the loss of double bond character and migration of hydrogen from substrate carbon (C<sub>RH</sub>) to the terminal sulfur (S<sub>Mo</sub>). There was also a considerable elongation of the Mo-O<sub>eq</sub> bond as compared to other bond distances, indicating a weak metal-ligand covalent bonding [12]. Amongst the bond distances, listed in Table 3.1, the O<sub>eq</sub>-C<sub>RH</sub> bond was shown to change remarkably in the course of the reaction. In addition, the allocation of electrons around the central metal (Mo) increased the force of electrostatic repulsion between the metal and the equatorial oxygen (O<sub>eq</sub>). This was shown to lead to a shorter O<sub>eq</sub>-C<sub>RH</sub> bond. The Mulliken atomic charge on selected atoms was shown to give stress for the formation and breaking of bonds that existed during the reaction. The oxo and sulfido group possessed negative charges because of their unique electronegative nature [13]. The decreasing of a partial negative charge on S<sub>Mo</sub> was due to the abstraction of a proton from (C<sub>RH</sub>) by the action of terminal sulfur and delocalization of the bonding pair of electrons between S<sub>Mo</sub> and Mo to the molybdenum center. The decreasing of partial positive charge on Mo was due to the accumulation of

negatively charged particles in the reduced state of Mo (Mo<sup>IV</sup>). On the contrary, the partial positive charge on carbon (C<sub>RH</sub>) decreased due to the formation of positive charge at the carbon atom during the migration of hydrogen to the terminal sulfur. This led to a decrease in partial negative charge on equatorial oxygen. In the course of the reaction, the partial positive charge on the transferred hydrogen atom (H<sub>RH</sub>) was found to decrease. Particularly, at the transition state (C) of ACT-D FA and ACT-P FA, the Mulliken charge on the hydrogen atom to be transferred was +0.016323 and -0.028500 a.u., respectively. The protonation of formaldehyde led to an increase the partial negative charge on H<sub>RH</sub> by -0.044823 a.u. Therefore, the protonation of formaldehyde had different connotations on the path of electrons transferred at the transition state. Furthermore, in both cases (ACT-D FA and ACT-P FA), the opposite charge on O<sub>eq</sub> and C<sub>RH</sub> indicated the nucleophilic and electrophilic nature of O<sub>eq</sub> and C<sub>RH</sub>, respectively. As a result, a nucleophilic addition reaction took place during the binding stage of the reaction. On the basis of the calculated data, the nucleophilic addition of the catalytically labile oxygen (O<sub>eq</sub>) of the active site to formaldehyde led to a stable intermediate. This intermediate was anticipated to undergo a hydride-transfer reaction with a low activation energy of about -0.019445kcal/mol (Fig.3.1). The % Mo<sub>oxy</sub> for the optimized geometries was shown in Fig.3.2.

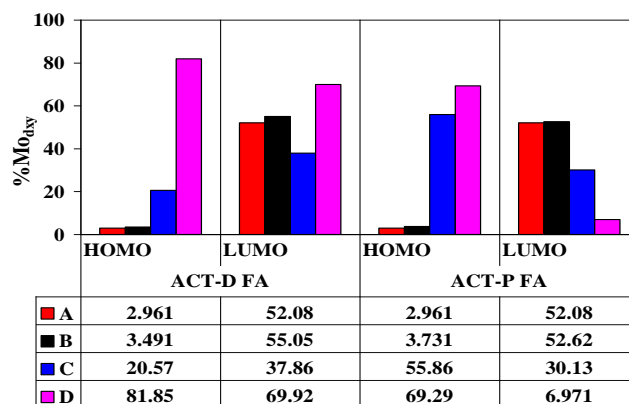


Fig.3.2: A plot of the % contribution of the molecular orbital fragments ( $\text{Mo}_{\text{dxy}}$ ) to the highest occupied molecular orbitals (HOMOs) and lowest unoccupied molecular orbitals (LUMOs) for the optimized geometries obtained as described in Fig.1.2.

The percentage contribution of the metal ( $\% \text{Mo}_{\text{dxy}}$ ) was increased during the course of the reaction. There was a small increment of  $\% \text{Mo}_{\text{dxy}}$  (2.961% to 3.491%) during the binding stage. Insignificant bond distance, Mulliken atomic charge, and % contribution change were observed during the binding stage (Table 3.1 and Fig. 3.2). Note that the coordination number of the molybdenum center remained unchanged in the course of the nucleophilic attack [12]. Interestingly, there was a significant molybdenum d orbital contribution (~52%) to LUMO in the binding stage (A) and substrate-bound structure (B) as compared to other intermediates and species. This means, the oxidation was supposed to be

Mo-based and electrons were more prone to shuttle between Mo and substrate [13]. The sulfido orbitals contribute ~33% to LUMO which implied that the electronic delocalization was also possible through sulfur during catalytic oxidation of substrates [13]. On the other hand, the remarkable increment of  $\% \text{Mo}_{\text{dxy}}$  (3.49% to 20.57% and from 20.57% to 81.85%), revealed the transfer of electrons from the substrate (FA) to the molybdenum center of the active site (AO). Similarly, the frontier orbitals for the optimized geometries, with the corresponding energy levels were shown in Fig.3.3.

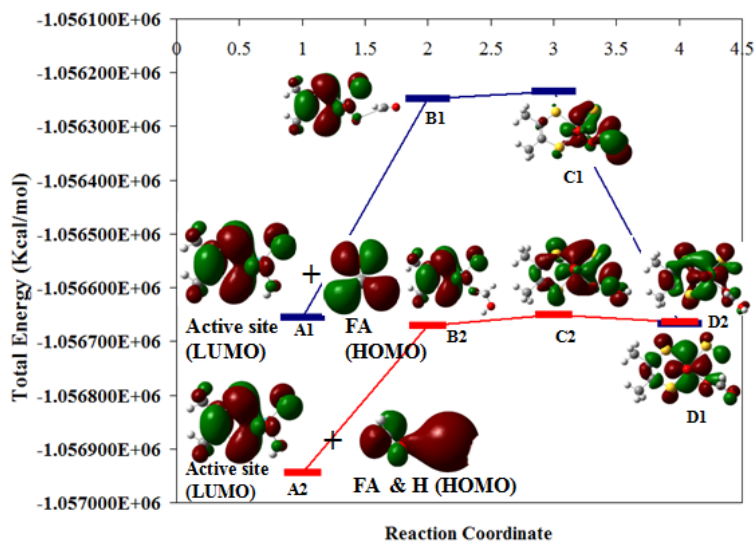
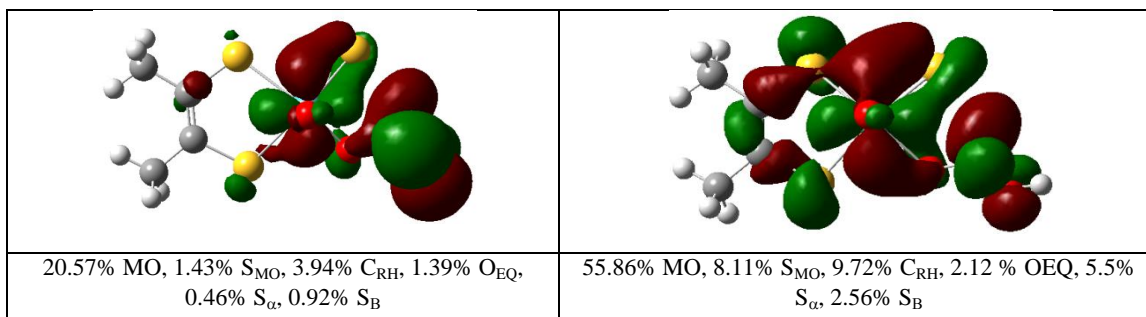


Fig 3.3: The wave function and energy levels description for structures (A-D).

In the binding stage (A), there was less accommodation of electrons to molybdenum as compared to other ligands coordinated to the metal, and thus revealed the readiness of the metal to accept electrons. The HOMO molecular orbital character of the active site was dominated by the contribution of p-orbitals of the two dithiolene sulfur ( $S_{\alpha}$  and  $S_{\beta}$ ) atoms. Therefore, the empty ( $\text{Mo}_{\text{dxy}}$ ) orbital of the active site accepted electrons from the substrate (FA). According to the frontier molecular orbital theory (FMO) of chemical reactivity, the Michaelis-Menten type (Enzyme)-[ $\text{Mo}^{\text{VI}}\text{-O-C}_{\text{CH}}$ ] complex (B) was formed as a

result of the interactions between highest occupied molecular orbital (HOMO) of the active site (AO) and lowest unoccupied molecular orbital (LUMO) of the substrates (FA) [14]. The less accommodation of electron densities observed on the substrate of the substrate bound intermediates (B1 and B2) indicated the partial transition of electrons from the substrate to the active site. Particularly, the frontier orbitals for the optimized geometries of the deprotonated (C1) and protonated (C2) transition state structures were shown in Fig.3.4.



**Fig.3.4:** The frontier molecular orbitals (HOMO) and % contributions of selected elements for the deprotonated ACT-D FA TS (C1) (*left panel*) and protonated HOMO-1 OF ACT-P FA TS (C2) (*right panel*) transition state structures.

As shown in Fig.3.4, the electron densities were highly accommodated at the metal center and on the substrate. However, there was less accommodation of electrons at the dithiolene sulfur atoms in the ACT-P FA TS (C2) as compared to ACT-D FA TS (C1) due to the intermixing of Mo and dithiolene sulfur orbitals. Therefore, the dithiolene sulfurs participate in buffering the electron density at the metal center [13]. The % contributions of chemical fragments (Mo, S<sub>Mo</sub>, C<sub>RH</sub>, O<sub>eq</sub>, S<sub>α</sub>, and S<sub>β</sub>) increased in the ACT-P FA TS as compared to ACT-D FA TS due to the protonation of formaldehyde. Furthermore, the higher % Mo<sub>dx<sub>y</sub></sub> (55.86%) on the protonated transition state structure was attributed to the increase in electron flow from the dithiolene sulfur and S<sub>Mo</sub> ligands. The smallest % contributions of other elements revealed that the fewer activities in the redox active sites of aldehyde oxidase. Interestingly, there was an increase in Mo d orbital contributions to LUMO in ACT-D FA TS (37.86% Mo) as compared to ACT-P FA TS (30.13% Mo). On the contrary, there was a significant lowering of Mo d orbital contributions to HOMO in ACT-D FA TS (20.57% Mo) as compared to ACT-P FA TS (55.86% Mo). This revealed that the oxidation was supposed to be Mo-based and electrons were more prone to shuttle between Mo and formaldehyde. Moreover, the sulfido terminal (S<sub>Mo</sub>) orbitals contributed 29.54% S<sub>Mo</sub> to LUMO in ACT-D FA TS as compared to ACT-P FA TS (0.350% S<sub>Mo</sub>). This implied the possibility of electronic delocalization through sulfur during catalytic oxidation of formaldehyde. Therefore, the catalytic oxidation of formaldehyde taken place on the deprotonated transition state (ACT-D FA TS). The calculated Moco model was

in line with [Mo<sup>VI</sup>(O)(S)(OH)(dt)]<sup>-a</sup> model that was employed in previous theoretical studies [13]. This observation further supported the hydride transfer associated with the sulfido terminal (S<sub>Mo</sub>) centers. The higher accommodation of electrons on the metal (Mo) center of product bound intermediates (D1 and D2) revealed the reduction of Mo from Mo<sup>VI</sup> to Mo<sup>IV</sup> as hydrogen moves from C<sub>RH</sub> to S<sub>Mo</sub> of the active site.

In general, the difference in % contribution to HOMO and LUMO frontier orbitals from each ligand was the indication of the electron density presence in their orbitals. The distribution of ligand orbitals to the metal center is due to the orbital overlapping taken place during the catalytic oxidation of formaldehyde. It also depended on the bonding (HOMO) and antibonding (LUMO) characters of the ligands, with respect to the metal ion.

## 2. Prediction and Characterization of the Transition State Structures

Since every reaction is expected to pass through the transition state, locating the transition state was the preliminary task in describing the reaction mechanism. The normalized energies with respect to the substrate bound Michaelis-Menten type complex were shown in Fig.3.5. The energies were used to locate the transition state and determine the energy barrier, for the reaction, during the catalytic oxidation of formaldehyde. The catalytic oxidation of formaldehyde was expected to pass either through the deprotonated (C1) or protonated (C2) transition states.

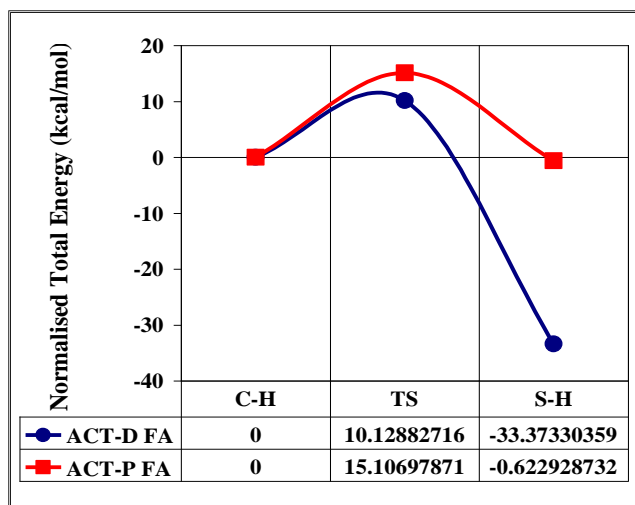


Fig.3.5: The normalized energies, for the active site bound to deprotonated formaldehyde (ACT-D FA) and protonated formaldehyde (ACT-P FA), plotted as a function of the reaction coordinates (C-H, TS, and S-H).

According to the data, the deprotonated transition state was lower in activation energy ( $\sim 10.13$  kcal/mol) than the protonated transition state ( $\sim 15.11$  kcal/mol). The energy difference between the substrate bound, transition state and product-bound structures for the catalytic oxidation of both deprotonated (*upper panel*) and protonated (*lower panel*) formaldehyde was shown in Fig.3.6. The protonated formaldehyde transition state was shown to bear a higher energy barrier. This was

shown to lead to the formation of a much less stable product with 372.89 kcal/mol (Fig. 3.6). This result indicated that this mechanism was not a likely mechanism [13]. As a result, the catalytic oxidation was shown to pass through the deprotonated formaldehyde transition state. Therefore, FA was kinetically and thermodynamically favorable for the formation of stable (Enzyme)-[Mo<sup>IV</sup>-O-C<sub>R</sub>] product.

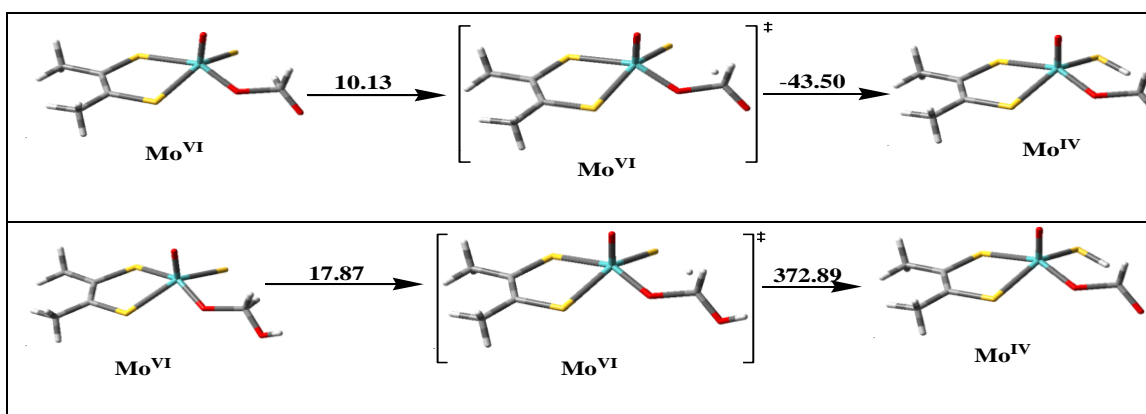


Fig.3.6: The energy barrier for the deprotonated (*upper panel*) and protonated (*lower panel*) substrate bound, transition state and product-bound structures.

This represents the actual transition state at which the reactant was transformed to the corresponding products. In addition, the electronic structure description for the deprotonated (C1) and protonated (C2) transition

state structure was characterized by one imaginary negative frequency, during the migration of H<sub>RH</sub> from C<sub>RH</sub> to S<sub>Mo</sub>. The frequency of ACT- D FA TS was higher than ACT-P FA TS, as shown in Fig.3.7.

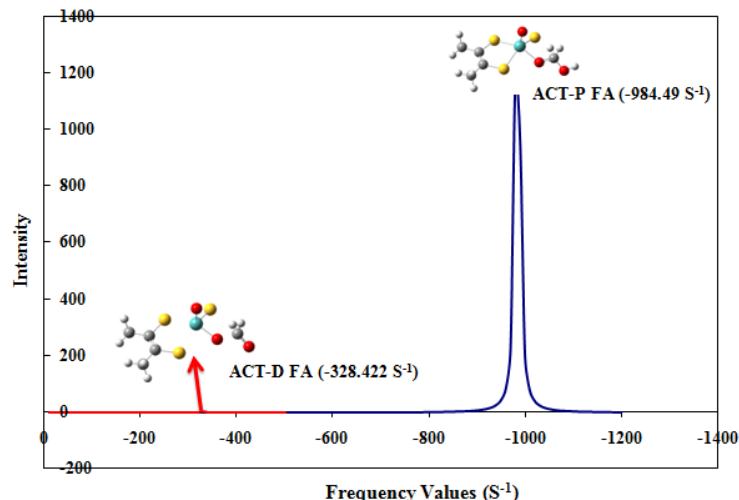


Fig.3.7: The plot of frequency values obtained from frequency calculations for the transition state (TS) structure. The intensity of peaks shown by red and blue colors (from left to right), respectively, were ACT-D FA and ACT-P FA.

The higher vibrational frequency of ACT-D FA TS revealed that the time required to pass the barrier of the reaction was small as compared to ACT-ACT-P FA TS. This enabled the conversion of reactants to the corresponding products to be faster. However, the intensity (degree of vibrational frequency) of ACT-P FA TS was higher as compared to ACT-D FA TS. This

phenomenon was correlated with the normalized energy profile shown in Fig.3.5 and thus revealed the kinetic feasibility of ACT-D FA TS compared to ACT-P FA TS. The %Mo<sub>dxy</sub> to the highest occupied molecular orbital (HOMO) of ACT-P FA and ACT-D FA bound to the active site was shown in Fig.3.8.

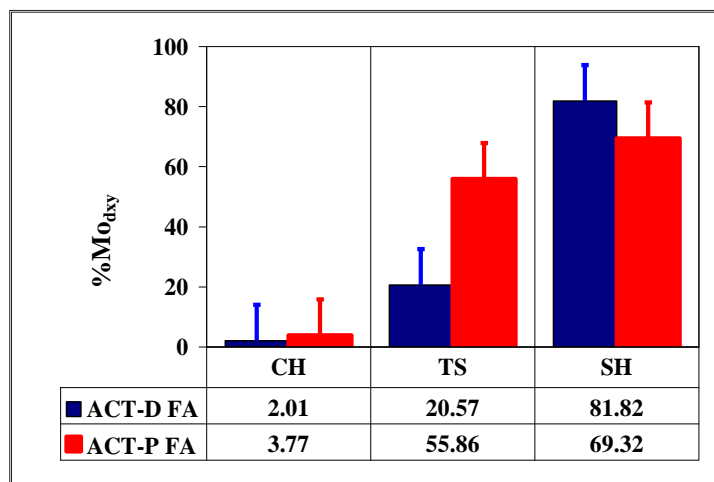


Fig. 3.8: A plot of % contribution, of the molecular orbital fragments (Mo<sub>dxy</sub>) to the highest occupied molecular orbital (HOMO) of ACT-D FA and ACT-P FA, as a function of reaction coordinates (CH, TS, and SH).

In both cases, the % contributions of molybdenum increased during the catalytic oxidation of formaldehyde due to the allocation of electrons around molybdenum

upon the reduction of Mo from Mo<sup>VI</sup> to Mo<sup>IV</sup>. The % Mo<sub>dxy</sub> to HOMO obtained from the linear transit calculation was shown in Fig.3.9.

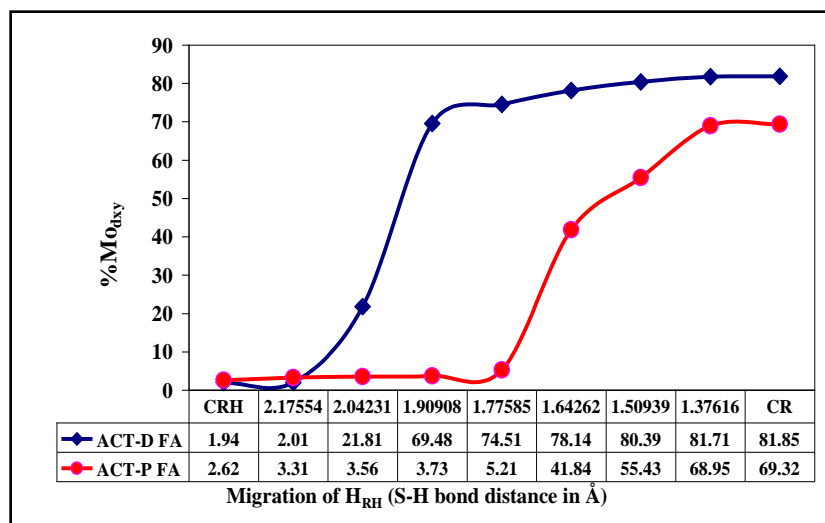


Fig 3.9: A plot of % contribution of the molecular orbital fragments ( $Mo_{dxy}$ ) to the highest occupied molecular orbital (HOMO) of ACT-D FA TS (upper trace) and ACT-P FA TS (lower trace) bound to the reductive active site of AO as a function of S-H bond distances in angstrom. The data was obtained from linear transit calculation during migration of  $H_{RH}$  from  $C_{RH}$  to  $S_{Mo}$ .

As shown in Fig.3.9, the % contribution of  $Mo_{dxy}$  increased during the migration of hydrogen ( $H_{RH}$ ) from substrate carbon ( $C_{RH}$ ) to the terminal sulfur ( $S_{Mo}$ ) due to the transfer of electrons to the molybdenum and hence the reduction of Mo from  $Mo^{VI}$  to  $Mo^{IV}$ . Particularly, a significant % contribution of  $Mo_{dxy}$  was observed in the catalytic oxidation of FA proceeding through the ACT-D FA TS (upper trace) as compared to ACT-P FA TS (lower trace). The % contribution of terminal sulfur ( $S_{Mo}$ ) also increased during the migration of hydrogen ( $H_{RH}$ ) due to the accepting ability of  $H_{RH}$  towards itself. As a result, the protonation of formaldehyde on the transition state had a considerable effect in the catalytic oxidation of formaldehyde.

**Characterization of the transition state using Mulliken atomic charges:** The atomic charge ( $\Delta q$ ) on Mo decreased from 0.630913 to 0.402641 a.u., during the migration of  $H_{RH}$  from  $C_{RH}$  to  $S_{Mo}$ , due to the allocation of electrons around it. The decrease of  $\Delta q$  on  $O_{eq}$  from -0.582462 to -0.43702 a.u. attributed to the absence of electrons expected to pass through it. Instead, the electrons destabilized the  $C_{RH}-H_{RH}$  bond, leading to the migration of  $H_{RH}$  to the terminal sulfido ( $S_{Mo}$ ), by increasing the partial positive charge on  $C_{RH}$ . The partial negative charge on  $S_{Mo}$  also decreased from -0.628706 to -0.393126 a.u., due to the delocalization of electrons from the  $Mo=S$  bonding electrons. The delocalization might occupy the empty  $d_{xy}$ -orbital of Mo, leading the decrease of the partial positive charge (increasing partial negative charge) on Mo. The decreasing of  $\Delta q$  on  $O_{eq}$  and increasing of  $\Delta q$  on  $H_{RH}$ , during the catalysis stage of catalytic oxidation of formaldehyde, revealed the path of electrons across the transferred hydrogen ( $H_{RH}$ ) rather than the equatorial

oxygen ( $O_{eq}$ ). Therefore, electron transfer followed the outer sphere mechanism ( $C_{RH}\dots H_{RH}\dots S_{Mo}\dots Mo$ ) rather than the inner sphere mechanism ( $C_{RH}\dots O_{eq}\dots Mo$ ). Moreover, there was negligible charge distribution in the apical oxygen ( $O_{ap}$ ) along the reaction path. Therefore, the oxo oxygen might likely act as a “spectator” group in this reaction.

In summary, as the data from the energy barrier, atomic charges, bonding descriptions, and molecular orbital analysis revealed, the deprotonated transition state structure was the favored path during the catalytic oxidation of formaldehyde. In addition, the electron transfer was shown to follow an outer sphere mechanism supported by hydride transfer.

### 3. Stepwise Mechanistic Route Leading to the Product Species

Different questions were also raised regarding the type of product generated (in the form of formate ion or formic acid) during the catalytic oxidation of formaldehyde. Different mechanistic routes (Path IA, Path IB, Path IC, and Path ID) were developed as shown in Fig.1.3.

In Path IC, the calculated activation energies associated with the removal of proton and electron from the structure (D1) to very rapid  $Mo^V$  structure (F and F') were 263.267 kcal/mol. These structures also exhibited similar % contributions to HOMO (Fig.3.10), atomic charge and bond order between chemical fragments (Table 3.2). The unique energy change, atomic charge, bond order, and % contribution between two structures insured the existence of resonance stabilization between them, as a result of the delocalization of lone pair and bonding pair of electrons from  $O_{eq}$  to  $C_{RH}$  and  $C_{RH}-O$  double bond, respectively. The increased in  $Mo-S_{Mo}$

bond order by 0.892 was shown to increase the partial positive charge on Mo (by 0.0912 a.u) and partial negative charge on  $S_{Mo}$  (-0.219956 a.u). This variation between structures (D1) and (F) indicated the development of  $\pi$ -bond between Mo and the terminal sulfur ( $S_{Mo}$ ) with subsequent removal of proton and electron. The negligible change in atomic charge and bond order of equatorial ligand observed between the two structures (D1 and F) (Table 3.2) also showed the inexistence of bond breaking and forming across the equatorial ligand coordinated to the central metal (Mo). The normalized energy associated with the binding of water to the resonance stabilized  $Mo^V$  structure (F') was

shown to -47310.733 kcal/mol. This led to the formation of water coordinated  $Mo^{VI}$  structure (I) and formate ion ( $HCOO^-$ ). Finally, the energetically stable  $Mo^{VI}$  structure (J) was regenerated. Although, formic acid ( $HCOOH$ ) was released as a result of proton abstraction from the water coordinated  $Mo^{VI}$  intermediate (I) with the minimum energy of -47355.733 kcal/mol. The increasing of Mo- $S_{Mo}$  bond order and subsequent increasing the partial charge of Mo during the course of the reaction indicated the regeneration of the active site. The frontier orbital and %  $Mo_{dxy}$  to HOMO (Fig.3.10) descriptions also supports the previous descriptions.

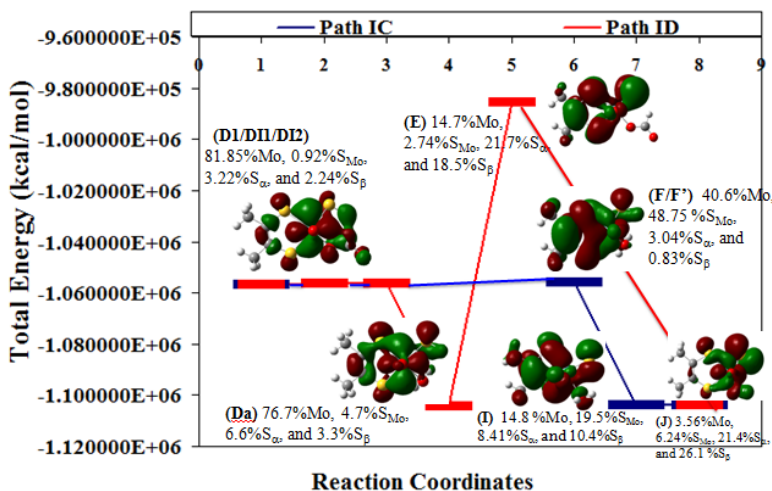


Fig.3.10: The plot of total energy obtained from the optimization of structures. The upper and lower trace indicated Path ID and Path IC, respectively.

As shown in the figure, the electrons were highly accommodated towards the active site and significant % contribution change was observed on the central metal

(Mo). Therefore, the catalytic oxidation of formaldehyde by aldehyde oxidase was molybdenum dependent.

Table 3.2: The Bond Orders and Mulliken Atomic Charge of Those Atoms (Mo,  $S_{mo}$ ,  $O_{eq}$ ,  $C_{RH}$ , And  $O_s$ ) Which Were Involved in the Formation and Breakage of Bonds During the Deprotonation of Formaldehyde for the Stepwise Mechanistic Route Leading to the Product Species.

Bonding pairs	Bond Order						
	D1	DI1/DI2	F/F'	Da	I	E	J
Mo- $S_{Mo}$	1.236	1.236	2.128	1.125	2.509	2.509	2.343
Mo- $O_{eq}$	0.714	0.714	0.776	0.491	0.321	0.321	1.150
$O_{eq}$ - $C_{RH}$	1.761	1.761	1.694				
$C_{RH}$ - $O_s$	2.220	2.220	2.249				
Elements	Mulliken Atomic charges						
Mo	0.396114	0.402221	0.487295	0.364917	0.486300	0.483871	0.609532
$S_{Mo}$	-0.394296	-0.393873	-0.614252	-0.344711	-0.301108	-0.170198	-0.416317
$O_{eq}$	-0.439784	-0.436947	-0.456116	-0.404562	-0.377531	-0.401688	-0.587425
$C_{RH}$	0.263716	0.265867	0.311032				

$O_s$	-0.458310	-0.462918	-0.446921				
-------	-----------	-----------	-----------	--	--	--	--

In the second Path (Path ID), the normalized energy associated with the formation of intermediate structures (DI1 and DI2), respectively were shown to be 263.267 and 265.267 kcal/mol. The similar atomic charge and bond orders (Table 3.2) between three structures (D1, DI1, and DI2) indicated the formation of resonance stabilization with the alteration of the position of electrons rather than the position of nuclei. Moreover, the normalized energy associated with coordination of water to the resonance stabilized intermediate (DI2) was shown to -47746.733 kcal/mol. This led to the formation of water coordinated  $Mo^{IV}$  structure (Da) and the release of formate ion. As shown in Fig.3.10, the unique %  $Mo_{dxy}$  contributions to HOMO (81.85%) of intermediate structures (D1, DI1, and DI2) and small %  $Mo_{dxy}$  change (by 5.15%) during the conversion of (DI2) to (Da) indicated the inexistence of oxidation reactions. However, significant %  $Mo_{dxy}$  change (by 61.9%) contributions during the conversion of structure (Da) to (E) was due to the loss of an electron and hence the oxidation of Mo from  $Mo^{IV}$  to  $Mo^V$ . The normalized energy associated with the removal of protons and the loss of electrons during the conversion of structure (E) to (J) was shown to be 71018.867kcal/mol. As shown in Table 3.2, the increasing of Mo- $S_{Mo}$  bond orders by 1.273 during the conversion of structure (Da) to structure (E) indicated the formation of  $\pi$ -bond between molybdenum and the terminal sulfur ( $S_{Mo}$ ) and thus behaved similar to structure (I) due to the similar % contributions of Mo ( $Mo_{dxy}$ ) to HOMO (Fig. 3.10). Therefore, Path ID was not the favored path and was thermodynamically infeasible due to the higher energy of structure (E) and other parameters. In general, Path IC was the most favored path due to the reasonable change in atomic charge, bond orders, frontier orbitals, percentage contribution, and reasonable minimum energy curve obtained during the catalytic oxidation of formaldehyde for the formation of the product (formic acid).

In the previous studies, Ilich *et al.* (2005) [7], proposed the existence of simultaneous nucleophilic addition reaction followed by hydride transfer before the transition state (early transition state). However,

Voityuk *et al.* (1998) [14], [15] suggested a stepwise pathway based on a model density functional study. In the previous studies, they found that the nucleophilic addition of the hydroxide on formaldehyde leads to a stable intermediate. This intermediate undergoes a hydride-transfer reaction with a low activation energy of about 7.7kcal/mol. Nevertheless, this result was not in line with our calculated data. Because, in the previous studies, the carbonyl oxygen of the substrate was assumed to interact with the central metal (Mo) of the complex<sup>[7]</sup>. Instead, our results supported the existence nucleophilic addition reaction between the carbonyl carbon atom ( $C_{RH}$ ) of formaldehyde with the catalytically liable equatorial oxygen ( $O_{eq}$ ) of the active site as a result of the development of highly partial negative charge of  $O_{eq}$  and partial positive charge of  $C_{RH}$ . Therefore, formaldehyde was bound to  $Mo^{VI}$  before oxidation and formaldehyde binding may occur in the course of the nucleophilic attack of the hydroxo group as shown in Fig. 1.2. A proton-electron coupled transfer occurred during the migration of  $H_{RH}$  from the substrate carbon ( $C_{RH}$ ) to the sulfido terminal ( $S_{Mo}$ ) at the catalysis stage and thus assured the existence of late transition state hydride transfer during the catalytic oxidation of formaldehyde. The higher energy barrier (Fig. 3.1) was also exhibited between structure (A) and (C), and thus reflected the existence of structure (B) between them. In addition, the formic acid product was released with a reasonable stepwise mechanistic pathway and minimum energy of -47355.89kcal/mol as shown in Fig.3.10. Therefore, the stepwise mechanism for the catalytic oxidation of formaldehyde by aldehyde oxidase was more favorable than the concerted mechanism.

Generally, Path IC was proposed as the most favored stepwise mechanistic pathway due to the reasonable change in energy, Mulliken atomic charge, bonding descriptions and molecular orbital analyses during the catalytic oxidation of formaldehyde. The proposed reaction mechanism for the catalytic oxidation of formaldehyde by the reductive half-reaction active site of aldehyde oxidase was shown in the following Fig.3.11.

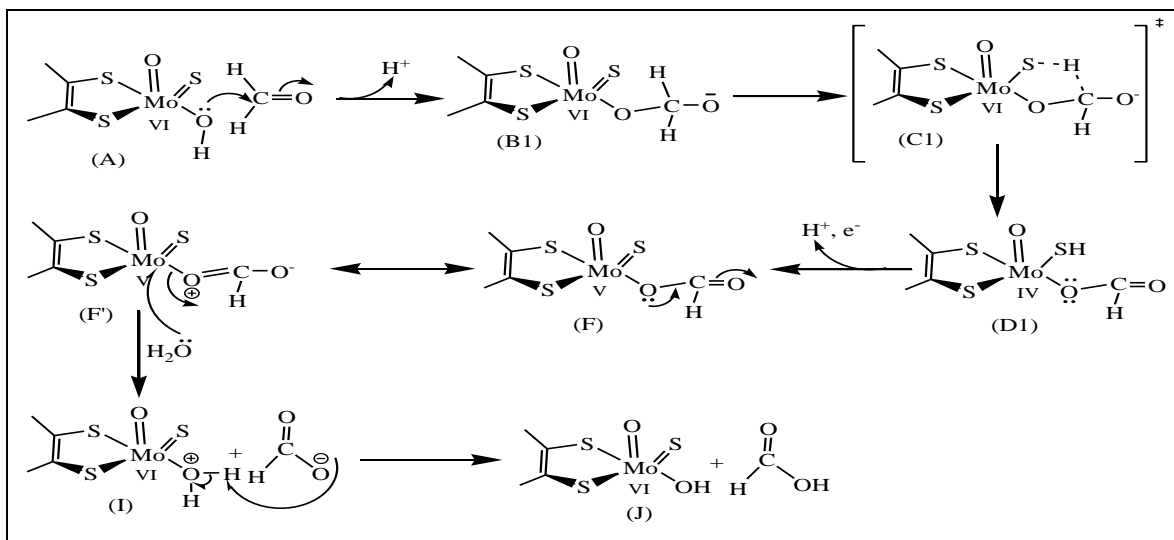


Fig.3.11: The proposed reaction mechanism for the catalytic oxidation of formaldehyde by the reductive half-reaction active site of aldehyde oxidase.

#### IV. CONCLUSION

In the present work, a DFT method and B3LYP level of theory have been employed for electronic structure calculation and quantum mechanical description of the transition state structure of formaldehyde bound to aldehyde oxidase enzyme.

Amongst the proposed reaction mechanisms, Path IC was the most favored path due to the reasonable change in atomic charge, bonding descriptions, and molecular orbital analyses, and reasonable minimum energy curve obtained during the catalytic oxidation of formaldehyde for the formation of the product (formic acid). On the other hand, formaldehyde inhibited structure might exist as IH<sub>2</sub> rather than H<sub>2</sub> due to the higher activation energy (224.002kcal/mol) during the transformation of the product bound intermediate (D1) to the inhibited Mo<sup>V</sup> structure (IH<sub>2</sub>). Moreover, the combined computation and experimental method of study would help to determine the formaldehyde inhibited aldehyde oxidase structure. Generally, a more general mechanism that followed stepwise process was probed for the catalytic oxidation of formaldehyde by aldehyde oxidase.

#### REFERENCES

- [1] Kisker, C., Schindelin, H., and Rees, D.C., (1997). Molybdenum-cofactor-containing enzymes: Structure and Mechanism. *Annu. Rev. Biochem.*, **66**, 233–267.
- [2] Mendel, R. R., (2007). Biology of the molybdenum cofactor. *J. Exp. Bot.*, **58**, 2289–2296.
- [3] Romao, M. J., (2009). Molybdenum and tungsten enzymes: A crystallographic and mechanistic overview. *J. Royal. Soc.*, **17**, 4053–4068.
- [4] Enroth, C., Eger, B.T., Okamoto, K., Nishino, T., Nishino, T., and Pai, E.F., (2000). Crystal structures of bovine milk xanthine

dehydrogenase and xanthine oxidase: Structure-based mechanism of conversion. *Proc. Nat. Acad. Sci.*, **97**, 10723–10728.

- [5] Hille, R., (2005). Molybdenum-containing hydroxylases. *Arc. Biochem. Biography*, **433**, 107–116.
- [6] Shinagawa, E., Toyama, H., Matsushita, K., Tuitemwong, P., Theeragool, G., and Adachi, O., (2006). A Novel type of formaldehyde-oxidizing enzyme from the membrane of *Acetobacter* sp. SKU. *Biosci. Biotechnol. Biochem.*, **70**(4), 850–857.
- [7] Zhang, X-H., Wu, Y-D., (2005). A Theoretical study on the mechanism of the reductive half-reaction of xanthine oxidase. *Inorg. Chem.* **44**, 1466–1471.
- [8] Yamaguchi, Y., Matsumura, T., Ichida, K., Okamoto, K., and Nishino, T., (2007). Human xanthine oxidase changes its substrate specificity to aldehyde oxidase type upon mutation of amino acid residues in the active site: Roles of active site residues in binding and activation of purine substrate. *J. Biochem.*, **141**, 513–524.
- [9] Mendel, R. R., Bittner, F., (2006). Cell biology of Molybdenum. *Biochimica et Biophysica Acta.*, **1763**, 621–635.
- [10] Schwartz, G., Mendel, R. R., and Ribbe, M. W., (2009). Molybdenum cofactors, enzymes, and pathways. *Nature*, **460**, 839–845.
- [11] Kulkarni, B., Tanwar, A., and Pal, S., (2007). Reactivity descriptors and electron density analysis for ligand chemistry: A case study of 2, 2'-bipyridine and its analogs. *J. Chem. Sci.*, **119**, 489–499.
- [12] J.A. People, Gaussian, Inc., Pittsburgh, PA., (2003). Gaussian 03W Help Table of contents. (File:///D:/worksoft/gaussian03/G03help/G03help/g03help.htm2003-12-3).
- [13] Amano, T., Ochi, N., Sato, H., and Sakaki, S., (2007). Oxidation reaction by Xanthine Oxidase. Theoretical study of the reaction mechanism. *J. Am. Chem. Soc.*, **129**, 8131–8138.
- [14] Alfaro, J. F., and Jones, J. P., (2008). Studies on the mechanism of aldehyde oxidase and xanthine oxidase. *J. Org. Chem.*, **73**, 9469–9472.
- [15] Voityuk, A. A., Albert, K., Romao, M. J., Huber, R., and Roesch, N., (1998). Substrate oxidation in the active site of Xanthine Oxidase and related enzymes. A model density functional study. *Inorg. Chem.*, **37** (2), 176–180.